Surface Science 98 (1980) 493-504

North-Holland Publishing Company and Yamada Science Foundation

EMISSION SPECTROSCOPY ON TWO-DIMENSIONAL SYSTEMS

E. GORNIK, R. SCHAWARZ and G. LINDEMANN

Institut für Physikalische Elektronik, Technische Universität, Wien and Ludwig-Boltzmann-Institut für Festkörperphysik, Wien, Austria

and

D.C. TSUI

Bell Laboratories, Murray Hill, New Jersey 07974, USA

Received 20 July 1979; accepted for publication 3 September 1979

Emission from subbands in inversion layers on (100) Si surfaces is investigated with narrow-band filters in combination with a Ga: Ge detector. Subband transition energies are determined over a wide range of electron densities and evidence for $1' \rightarrow 0'$ transitions is given. Emission from electronic transitions between minigaps is studied with a GaAs and a tunable InSb detector. For the first time, the energy of higher minigaps is determined as a function of the electron concentration in the channel.

1. Introduction

The investigation of two-dimensional systems by spectroscopic methods has yielded detailed information on energy levels and effective masses in surface inversion and accumulation layers on Si. Most of the work has been performed by absorption, absorption derivative spectroscopy [1] and photoconductive techniques [2-4] using lasers. More recently Fourier transform spectroscopy has been successfully applied to studies of subband transitions [5], cyclotron resonance [6], minigap [7] and plasmon [8] phenomena on (100) Si surfaces.

The investigation of far infrared emission from Si MOSFETs on (100) surfaces, excited by current pulses through the channel, was first started from the aspect of tunable emission [9]. Since the subband splitting depends on the gate voltage, the emission frequency is voltage tunable. Besides the source aspects, which had its drawback in the extremely low intensities of $\sim 10^{-11}$ W, this tunability opened the possibility for a quite simple spectroscopy; the emitted radiation is tuned through narrowband filters, which allows, in combination with a broadband detector, an analysis of the radiation. This spectroscopy is equivalent to absorption spectroscopy with lasers, since in both cases the energy levels are tuned through a defined energy.

Besides the subband emission, radiation due to several other electronic processes in Si MOSFETs, namely cyclotron emission [10], minigap emission [11] and the radiative decay of two-dimensional plasmons [12] has been reported. In these cases, a narrowband extrinsic GaAs detector served as a filter and detector at the same time and spectroscopy is again performed by sweeping the gate voltage. However, this technique is not complementary to a direct frequency analysis of the radiation under fixed external perturbation. Since the emission intensities are quite low, so that an external frequency analysis by a spectrometer would be too time consuming, we applied a tunable n-InSb detector [13,14] to perform a direct frequency analysis of the radiation. The n-InSb detector can be continuously tuned from 3 to \sim 20 meV with a magnetic field. The detector linewidth is about 3 cm⁻¹ at 2 K yielding a reasonable resolution. This technique has its potential applications when the resonance cannot be swept by an external perturbation or when the emission tunes very slowly with gate voltage.

In the following review, we want to demonstrate the capability of the emission spectroscopy. The narrow band filter technique is applied to a series of Si MOSFETs on (100) surfaces with oxide thicknesses as varying between 1200 and 13000 Å and channel lengths between 40 μ m and 2.5 mm. Four different absorption filters in the energy range between 10 and 25 meV are used and detailed information on subband energies is obtained.

The tunable spectroscopy with n-InSb is applied to a study of the minigaps. Optical transitions across minigaps are observed in samples tilted 1.1° from the (100) surface. For the first time, information on the gate voltage dependence of higher minigaps is given.

2. Experimental methods

The radiation is generated by voltage pulses applied between the source and drain contacts of the MOSFETs. The electron distribution in the channel is heated and higher levels (or excitations) are occupied leading to partial radiative decay. The emitting MOSFET is mounted inside a brass light pipe opposite to the detector. Different geometric arrangements and detection techniques are used depending on the emission process to be observed.

2.1. Subband emission

The radiation is linearly polarized perpendicular to the interface and therefore emitted parallel to the interface. The device is mounted with the interface oriented in the direction of the detector. A (\sim 1 μ m) Au or Al metallization is deposited on the gate electrode. This gate metallisation provides defined boundary conditions for the radiation and "shortcircuits" the blackbody thermal radiation from the hot electron gas in the channel. The amount of blackbody radiation can be determined

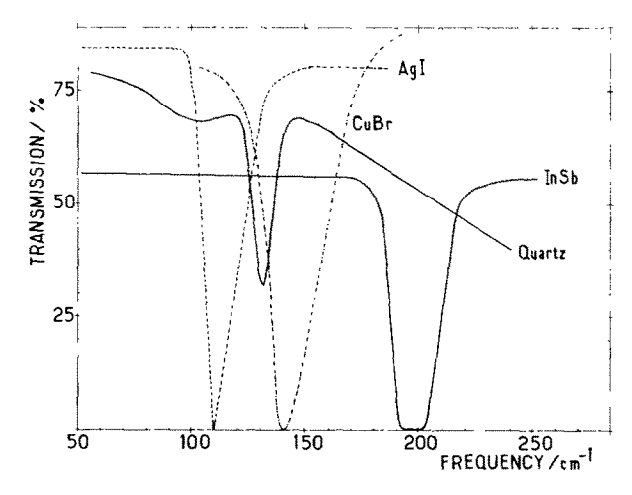


Fig. 1. Transmission characteristics of several materials at 4.2 K as a function of frequency.

on samples with a semitransparent gate to be about 10 times higher than the subband emission, thus masking subband emission completely. Since the channel is a very thin sheet of electrons, this radiation is only emitted perpendicular to the interface. A metal in the near field of the channel can therefore short-circuit this radiation. Moreover, the substrate side of the device is also metallized to provide an efficient guiding of the radiation.

The emitted radiation is detected and analysed with a broadband Ga doped Ge

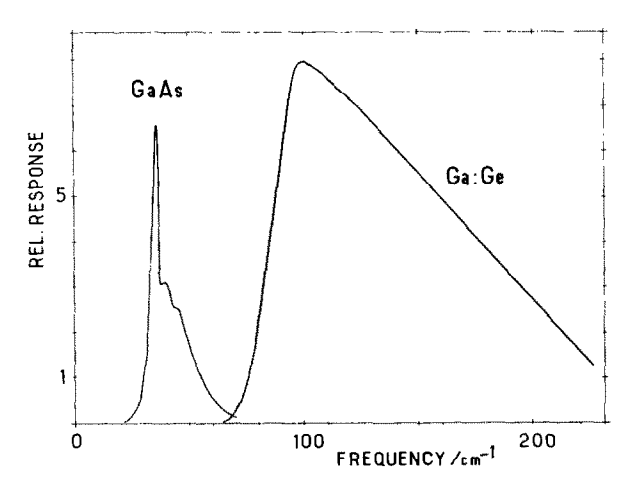


Fig. 2. Relative detector response of a photoconductive n-GaAs and Ga doped Ge detector as a function of frequency at 4.2 K (resolution 1 cm⁻¹).

detector [15] in combination with several narrowband filters inserted between detector and emitter. In the experiment the detector signal is measured as a function of gate voltage. The transmission characteristics of the filters used at 4.2 K are shown in fig. 1. AgI [16] and CuBr [17] are reststrahlen filters made of powder suspended in glue and deposited on mylar with a thickness of a few μ m. The quartz filter is made of 2 mm crystalline quartz [18], while the InSb filter also used as reststrahlen filter is a platelet of 100 μ m thickness cut from a high purity single signal. The frequency response of the Ga: Ge detector is shown in fig. 2. The detector has a rather sharp cut off at 80 cm⁻¹ and is sensitive to about 300 cm⁻¹.

2.2. Emission perpendicular to the interface

For emission processes, with the polarization vector in the plane of the interface the radiation is emitted perpendicular to the interface. These processes include the cyclotron [10], the minigap [11] and the plasmon [12] emission. To observe these processes a semitransparent gate has to be used. A better coupling out of the radiation from Si is achieved by glueing the devices on a 12.5 cm diameter Si halfsphere. This arrangement has the drawback that the blackbody radiation from the hot electron gas is also observed. However, all the above mentioned emission processes are at least of the same intensity as the broadband emission so that a separation is possible. The samples are mounted in a light pipe with the emission directed to the detector. In most of the previous experiments [10-12] a narrow-band GaAs detector was used to analyze the radiation by sweeping the gate voltage. The emitted frequencies are in the range between 10 and 80 cm⁻¹ and thus outside the range of the Ga: Ge detector. The frequency response of the n-GaAs detector is shown in fig. 2. In a magnetic field the dominant 1s-2p line of GaAs splits into 3 lines [19] and one line (1s-2p, m=+1) shows a strong tunability with the field. However, this detector can not be effectively used as magnetic field tunable spectrometer since the photoconductivity spectrum consists always of all three lines. In addition, the response of the detector decreases considerably with magnetic field. To obtain information on the frequency spectrum of the emitted radiation we used a magnetic field tunable n-InSb detector. InSb can be used as spectrometer in the frequency range between 20 and 155 cm⁻¹ (corresponding to 2.5 and 19 meV). Fig. 3 shows the frequency response of the n-InSb detector as a function of magnetic field for several frequencies at 2 K; it consists of one line which shifts linearly with magnetic field. The photoconductive response of n-InSb in a magnetic field consists basically of two lines, the cyclotron resonance line and the so called impurity shifted cyclotron resonance line. At temperatures well below 4.2 K the response is dominated by the impurity line since the conduction band is depopulated due to freeze out. The resolution of n-InSb at 2 K is in the order of 3-4 cm⁻¹. A drawback of this detector is its lower sensitivity compared to the Ga: Ge detector (about 2 orders of magnitude lower). However, this detector can be successfully applied to the analysis of far infrared radiation.

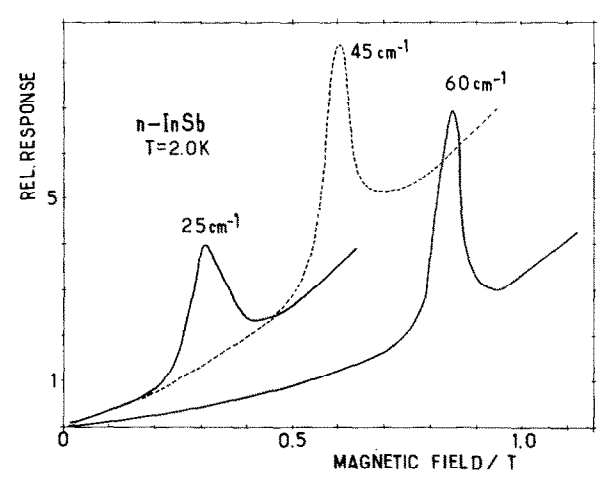


Fig. 3. Relative response of a tunable n-InSb detector as a function of magnetic field for 3 incident frequencies at 2.0 K.

3. Subband emission

Subband emission experiments have been performed on (100) Si n-channel MOSFETs [9,10,20]. A rather small range of energies between 12.5 and 16.5 meV has been investigated. Besides the spectral analysis of the radiation with the help of transmission filters (As doped Ge and crystalline quartz) the electric field dependence of the emission intensity for the $1 \rightarrow 0$ transition [9] (transition between the lowest two subbands) and the electron temperature in the channel as a function of the channel electric field [20] have been determined. The problem of establishing electrostatic equilibrium has been recognized. It was found that the resulting depletion charge N_{depl} can be varied actually between 0 and the full charge given by the bulk doping by cool down conditions [10]. The main problem with emission investigations comes from the fact that rather high channel fields are required to heat the electron gas sufficiently. This leads to an inhomogeneous electron distribution along the channel in large area devices. Two approaches were used to overcome this problem. On the one hand, the oxide thickness was increased up to 1.3 μ m, which allowed the application of higher channel fields and an analysis of the radiation down to lower densities. On the other hand, devices with considerably shorter channel length (40 μ m) and large width of the channel (2 mm) were used.

Fig. 4 shows emission spectra from a 2.5×2.5 mm² gate area MOSFET device ((100) surface) with an oxide thickness of 1.0 μ m. The device was fabricated at Bell Laboratories and had a peak effective mobility of 18.000 cm²/V·s at 4.2 K. A CuBr filter with a resonant absorption at 17.6 meV and an InSb filter with the reststrahlen band at 24.0 meV were used for frequency analysis. With the InSb

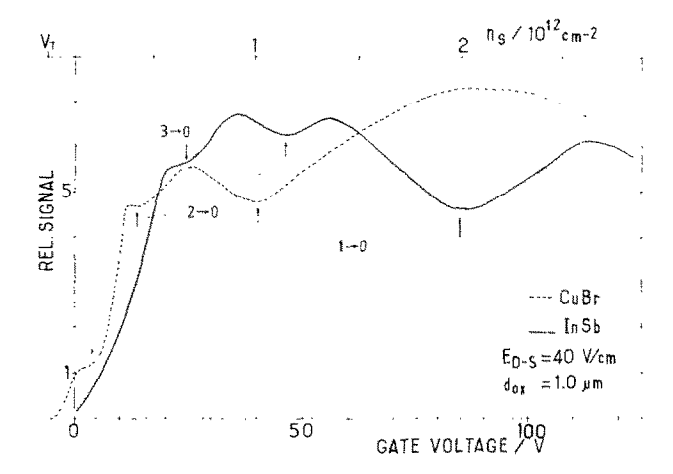


Fig. 4. Emission signal detected with a Ga: Ge detector as a function of gate voltage (and n_8) for a MOSFET with $d_{OX} = 1.0 \, \mu \text{m}$ as observed through narrowband filters at 4.2 K; (·····) CuBr, (——) InSb. The minima are assigned to different subband transitions. The dashed arrow indicates a $1' \rightarrow 0'$ transition (see text).

filter 3 subband transitions are resolved clearly as minima, the transition $1 \rightarrow 0$ and 2 transitions from higher excited states to the ground state. This observation reflects more or less the transition probability differences between the different levels. In the emission experiment the gate voltage is swept at constant channel field and every transition is excited with the same efficiency since the transition is observed when it equals the filter energy.

The widths of the observed minina are getting narrower going from transition $1 \rightarrow 0$ to $3 \rightarrow 0$ indicating a stronger frequency on gate voltage dependence with increasing number of the excited state. The spectrum observed with the CuBr filter reveals 2 clearly resolved lines due to $1 \rightarrow 0$ and $2 \rightarrow 0$ transitions and some additional structure at low densities, which will be discussed later.

A comparison of spectra obtained with MOSFETs on (100) surfaces from different sources using a AgI filter in combination with the Ga: Ge detector is given in fig. 5. Curve (a) shows the emission intensity of a "Siemens" sample with an oxide thickness of 1200 Å, a peak mobility of 6000 cm²/V · s (at 4.2 K) and a channel length of 40 μ m (channel width 2 mm). The channel voltage applied is 0.7 V corresponding to an electric field of 175 V/cm. Curve (b) represents the spectrum of a "Hitachi" sample with an oxide thickness of 6000 Å and a gate area of 2 × 2 mm². The peak mobility is 16,500 cm²/V · s at 4.2 K. The electric field is 35 V/cm. Two lines are very clearly resolved and again some additional structure is observed at very low gate voltages. Curve (c) is obtained with a 1.3 μ m oxide "Bell Laboratories" sample with a gate area of 2.5 × 2.5 mm² and a peak mobility of 15,000 cm²/V · s. The channel field is 35 V/cm. The absorption minima are shifted to con-

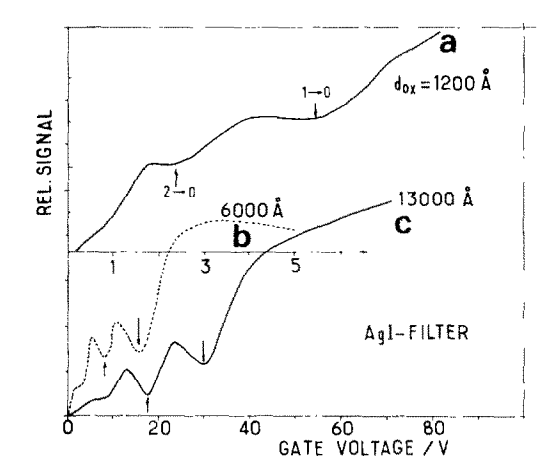


Fig. 5. Emission spectra detected with Ga: Ge as a function of gate voltage for 3 different MOSFETs through a AgI filter. (a) "Siemens" sample: oxide thickness 1200 Å, peak mobility $6000 \text{ cm}^2/\text{V} \cdot \text{s}$ (4.2 K), channel length 40 μm , channel width 2 mm; (b) "Hitachi" sample: oxide thickness 6000 Å, peak mobility $16,500 \text{ cm}^2/\text{V} \cdot \text{s}$ (4.2 K), gate area $2 \times 2 \text{ mm}^2$; (c) "Bell Laboratories" sample: oxide thickness $1.3 \mu\text{m}$, peak mobility $15,000 \text{ cm}^2/\text{V} \cdot \text{s}$ (4.2 K), gate area $2.5 \times 2.5 \text{ mm}^2$.

siderably higher gate voltages for the sample, the dips appear as clear as for the "Hitachi" sample. Several features are rather surprising on these results: a reasonable narrow emission line can be determined from the data on the rather low mobility Siemens sample. The linewidth found is about a factor of two larger than that of the other two samples, which does not scale with the peak mobility being a factor of \sim 3 lower. In addition, it has to be considered that the applied electric field and thus, the effective electron temperature are also considerably higher. However, this behaviour is consistent with absorption data [21] showing no linewidth increase with temperature up to 130 K. The observation that subband transitions can be analysed in emission up to rather high channel fields emphasizes the emission method to be superior to the absorption method for short channel devices. As the emission intensity is an exponential function of the channel field and as reduction in channel length leads to a linear decrease in intensity, it seems possible to investigate devices with channel lengths down to 10 μ m and below with the emission method.

The linewidth of the emission for the $1 \rightarrow 0$ and $2 \rightarrow 0$ transition is found to be in the order of 0.8 (± 0.2) meV at 13.65 meV in the higher mobility samples. However, the intensity of the $2 \rightarrow 0$ transition is about the same as the $1 \rightarrow 0$ transition when accounting for the lower density at which the equivalent frequency appears. At the position of the $2 \rightarrow 0$ transition the channel is rather inhomogeneous, for the drain-source voltages used. The application of a drain-source voltage comparable to the gate voltage will create a channel where the resistance of the channel varies

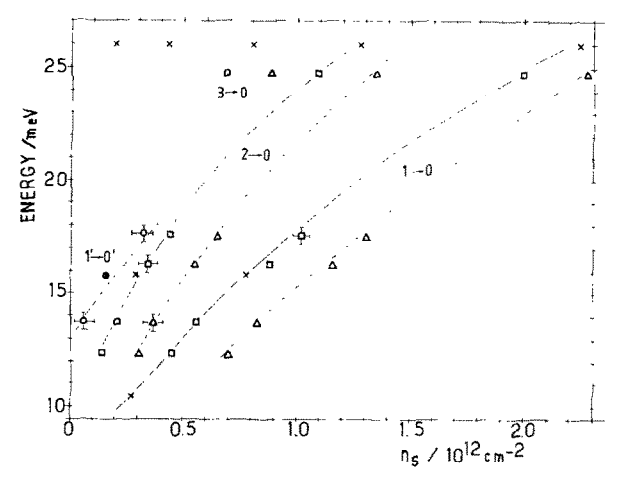


Fig. 6. Subband transition energies as a function of electron density (n_s) for a MOSFET with $d_{\rm OX}=1.0~\mu{\rm m}$. Two different $N_{\rm depl}$ are realized by cool down conditions [10]: $N_{\rm depl}=6\times10^{10}~{\rm cm}^{-2}~(^{\circ})$; $N_{\rm depl}=1\times10^{10}~{\rm cm}^{-2}~(^{\circ})$. The open circles indicate $1'\to0'$ emission for $N_{\rm depl}=6\times10^{10}~{\rm cm}^{-2}$; photoconductivity data by Neppl et al. [4] for $N_{\rm depl}=6.0\times10^{10}~{\rm cm}^{-2}$ are also included (X). The curves are fits to the experimental data.

considerably between drain and source. As a consequence, the electric field in the channel will not be constant. Most of the voltage will drop at the high resistivity side of the channel and create there a considerably higher field. This is likely the reason for the high intensity of the $2 \rightarrow 0$ transition. From the fact that the linewidth still remains rather narrow, we conclude that the voltage drops within a rather short distance and that the linewidth of the $2 \rightarrow 0$ transition does not increase significantly with electron temperature. Emission from other parts of the channel does not effect the line since the electric field and thus, the intensity is low.

A plot of transition energies as determined with a series of filters and the known detector response is shown in fig. 6 for a "Bell Laboratory" sample with an oxide thickness of $1.0 \, \mu \text{m}$. Two different depletion charge densities $N_{\text{depl}} \sim 6 \times 10^{10}$ cm⁻² and $N_{\text{depl}} \sim 1 \times 10^{10}$ cm⁻² were realized by different cool down conditions. In both cases, up to three subband transitions are observed. Photoconductivity data by Neppl et al. [4] from a sample with the same depletion charge ($N_{\text{depl}} \sim 6 \times 10^{10}$ cm⁻²) are included for comparison. The transition energies agree well with Ando's theoretical results [22] for the $1 \rightarrow 0$ transition for both depletion charges. However, the higher transitions are lower in energy than predicted by theory.

At low densities we observe an additional emission in the energy range between 13.5 and 18.0 meV, which has a considerably stronger electric field dependence than the $2 \rightarrow 0$ transition. The determination of the corresponding electron concentration is rather difficult due to the extremely inhomogeneous channel situation.

By investigating several positive and negative channel voltages we determined the two points for the AgI and CuBr filters marked by circles in fig. 6. Because of the strong channel field dependence we assign these energies to transitions between the fourfold degenerate set of subbands $1' \rightarrow 0'$. Kneschaurek et al. [21] have observed an additional absorption line at rather low densities at 15.7 meV which increased in intensity with increasing temperature. They interpreted this line as $0' \rightarrow 1'$ transition. The result of Kneschaurek et al. [21] is marked by the circle with the cross in fig. 6 and seems to fit the tendency given by the other two points. If we accept this interpretation, we have found the dependence of the $0' \rightarrow 1'$ transition energy as a function of density within a small concentration range. Ando [23] has calculated the dependence of the energy difference between the two ground levels of the two different sets of valleys $(0 \rightarrow 0')$ and has found about the same slope for the $0 \rightarrow 0'$ energy difference as for the $1 \rightarrow 0$ transition. We find a similar slope compared to the $1 \rightarrow 0$ transition (somewhat steeper) but a weaker slope as compared to the $2 \rightarrow 0$ transition. As the $3 \rightarrow 0$ transition would have an even steeper slope than the $2 \rightarrow 0$ transition, we conclude that the $3 \rightarrow 0$ transition cannot be responsible for the observed emission. Therefore, we believe that our data give evidence for $1' \rightarrow 0'$ transitions in the energy range between 13.6 and 17.6 meV.

4. Minigap emission

The two-dimensional band structure of electron inversion layers on surfaces tilted a few degrees from (100) exhibits one-dimensional energy gaps — "minigaps". Cole et al. [24] first observed these minigaps through an anomaly in the gate voltage dependence of the channel conductivity. Sham et al. [7] proposed the so-called "projection surface band model", which has been very successful in predicting the positions of the various gaps, which have been detected in the meantime by conductivity measurements [25,26] and by infrared spectroscopy [27,11]. In particular Tsui et al. [25] observed anomalies in the conductivity due to 4 minigaps in samples with small tilt angles ($\theta \leq 3^{\circ}$).

More recently, systematic spectroscopic investigations [31,32] on a series of samples with tilt angles between 1.1° and 12° have found empirical formula to describe the energy splitting of the lowest minigap (occurring at a Fermi vector $k_{\rm F} = (2\pi/a - k_0) \sin \theta$ [25], where a is the lattice constant of Si and $k_0 = 0.85(2\pi/a)$ is the value of the wave vector at the conduction band minima along the $\langle 100 \rangle$ directions).

We have performed emission experiments on series of samples tilted by 1.1° to 8.9° from [100] in a (110) plane. Fig. 7 shows the photoconductive response of a GaAs detector as a function of gate voltage for 3 samples. The 8.9° and 5.6° samples exhibit one resonant peak due to narrowband emission at 4.4 meV (resonant detector response at 4.4 meV, see fig. 2), the 2.9° sample reveals a second peak at higher gate voltages.

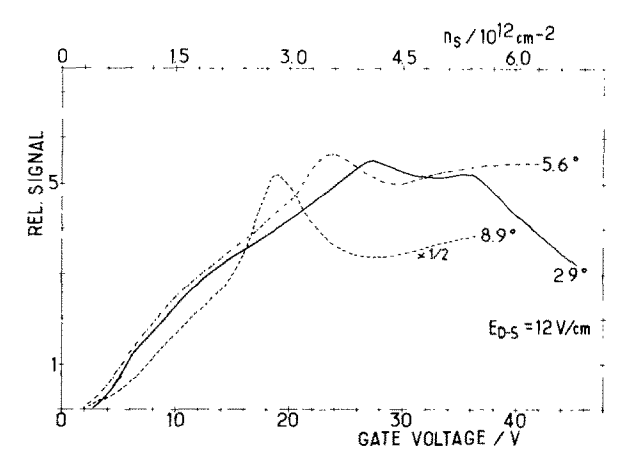


Fig. 7. Minigap emission spectra obtained with a n-GaAs detector as a function of gate voltage for MOSFETs with different tilt angles.

In the experiment with the GaAs detector the minigaps are tuned through the narrow detector line and a resonance is only observed if the size of the minigap coincides with the detector resonance in the sweep range. Minigaps below and above the detector line cannot be observed. The use of a tunable n-InSb detector avoids this disadvantage. However, due to its lower sensitivity, lower signal to noise ratios have to be accepted. With the n-InSb detector we investigated minigap splittings in a range between 2.5 and 8 meV. In the experiment we tune the resonant response of the InSb detector (shown in fig. 3) with the magnetic field and keep the channel concentration constant. We apply current pulses between drain and source to excite the emission. Fig. 8 shows emission spectra as a function of magnetic field measured with an n-InSb detector for a 1.1° sample and n_s values between 1 \times 10¹² and 6.9 × 10¹² cm⁻². At the lowest density no structure is observed, the detected signal is due to broadband hot electron emission. The sensitivity of the detector increases with magnetic field to an increasing detector resistance. With increasing density first two and at the highest density four maxima in the emission signal become visible. These maxima are due to narrowband emission at distinct frequencies. The positions of the peaks are marked by arrows. The frequencies which, according to our interpretation, belong to the same minigaps are combined by dashed lines.

In fig. 7, the 8.9° and 5.6° samples reveal only one minigap (lowest minigap) while the second resonance in the 2.9° samples gives evidence for a second minigap. The appearance of the second minigap in emission coincides with the anomaly in conductivity [25]. By comparison with the analysis of ref. [32], we assign the highest emission energy (appearing at the highest magnetic fields) to the minigaps at $k_F = (2\pi/a - k_0) \sin \theta$ which shows the strongest energy on gate voltage dependence. The assignment of the next minigaps is then straightforward. We find that

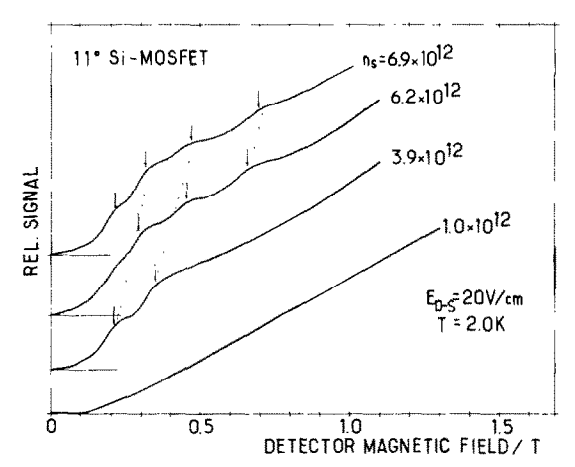


Fig. 8. Emission signal for an n-InSb detector as a function of magnetic field for a MOSFET with a tilt angle of 1.1° and several electron densities. The observed lines are indicated by arrows. The dashed lines indicate the frequency shift on the lines with n_s .

the energy splitting of the higher minigaps increases considerably weaker with gate voltage than that of the lowest one. For the 1.1° sample, we determined the second minigap to be 3.0 meV at $n_{\rm s}=2.5\times10^{12}~{\rm cm^{-2}}$ and to increase to 4.7 meV for $n_{\rm s}=6.9\times10^{12}~{\rm cm^{-2}}$. The third minigap is 2.3 meV for $n_{\rm s}=3.9\times10^{12}~{\rm and}$ 3.2 meV for $6.9\times10^{12}~{\rm cm^{-2}}$. The fourth minigap is only observed at the highest $n_{\rm s}$ value to be $\sim2.3~{\rm meV}$.

In addition, we have also studied the effect of substrate bias on the size of the minigap for a 8.9° and 6° sample. In these samples, only the lowest minigap is observed. We have changed $N_{\rm depl}$ between 1 \times 10¹⁰ and 6 \times 10¹¹ cm⁻² by applying substrate voltages between +0.3 V and -30.0 V. These investigations were performed by sweeping the gate voltage through the GaAs line. We found that the detector resonance corresponding to a minigap splitting of 4.4 meV, always appears at the same gate voltage and was independent of the substrate voltage. This indicates that the size of the minigap depends basically only on the surface field given by $F = (4\pi e^2/\epsilon_{\rm Si})(n_{\rm S} + N_{\rm depl})$ in contrast to theory [33-35] which predicts a dependence as

$$F = (4\pi e/\epsilon_{Si})(n_s + \gamma N_{depl})$$

with $\gamma = 32/11$.

Acknowledgement

Part of this work is supported by the Fonds zur Förderung der wissenschaftlichen Forschung (Schwerpunkt S22-5), Austria.

References

- [1] P. Kneschaurek and J.F. Koch, Phys. Rev. B15 (1977) 1590; and references therein.
- [2] C.C. Hu, J. Pears, K.M. Cham and R.G. Wheeler, Surface Sci. 73 (1978) 207.
- [3] A. Kamgar, D.C. Tsui and M.D. Sturge, Solid State Commun. 24 (1977) 47; Surface Sci. 73 (1978) 166.
- [4] F. Neppl, J.P. Kotthaus and J.F. Koch, Phys. Rev. B16 (1977) 1519; On the Mechanism of Intersubband Resonant Photoresponse, to be published.
- [5] B.D. McCombe and D.E. Schafer, in: Proc. Intern. Conf. on the Physics of Semiconductors, Edinburgh, Inst. of Phys. Conf. Series 43 (1979) 1227;
 B.D. McCombe, R.T. Holm and D.E. Schafer, Solid State Commun., to be published.
- [6] S.J. Allen, D.C. Tsui and J.V. Dalton, Phys. Rev. Letters 32 (1974) 107.
- [7] L.J. Sham, S.J. Allen, Jr., A. Kamgar and D.C. Tsui, Phys. Rev. Letters 40 (1978) 472.
- [8] S.J. Allen, Jr., D.C. Tsui and R.A. Logan; Phys. Rev. Letters 38 (1977) 980.
- [9] E. Gornik and D.C. Tsui, Phys. Rev. Letters 37 (1976) 1475.
- [10] E. Gornik and D.C. Tsui, Surface Sci. 73 (1978) 217.
- [11] D.C. Tsui and E. Gornik, Appl. Phys. Letters 32 (1978) 365.
- [12] R.C. Logan, E. Gornik and D.C. Tsui, Bull. Am. Phys. Soc. 24 (1979) 438.
- [13] E.H. Putley, Phys. Status Solidi 6 (1964) 571; J. Sci. Instr. 43 (1966) 857.
- [14] E. Gornik, W. Müller and F. Kohl, IEEE Trans. MTT22 (1974) 967.
- [15] W.J. Moore and H. Shenker, Infrared Phys. 5 (1965) 99.
- [16] A. Hadni, J. Claudel and P. Strimer, Appl. Opt. 7 (1968) 1159.
- [17] J.N. Plendl, A. Hadni, J. Claudel, Y. Henninger, G. Morlot, P. Strimer and L.C. Mansur, Appl. Opt. 5 (1966) 397.
- [18] E.V. Loewenstein, D.R. Smith and R.L. Morgan, Appl. Phys. 12 (1973) 398.
- [19] G.E. Stillman, C.M. Wolfe and S.D. Dimmock, Solid State Commun. 7 (1969) 921.
- [20] E. Gornik and D.C. Tsui, Solid State Electron. 21 (1978) 139.
- [21] P. Kneschaurek and J.F. Koch, Phys. Rev. B16 (1977) 1590.
- [22] T. Ando, Solid State Commun. 21 (1976) 133.
- [23] T. Ando, Phys. Rev. B13 (1976) 3468.
- [24] T. Cole, A.A. Lakhani and P.J. Stiles, Phys. Rev. Letters 38 (1977) 722.
- [25] D.C. Tsui, M.D. Sturge, A. Kamgar and J.J. Allen, Jr., Phys. Rev. Letters 40 (1978) 1667.
- [26] W. Sesselmann, T. Cole, J.P. Kotthaus, R. Kellerer, H. Gesch, J. Eisele, G. Dorda and P. Goy, in: Proc. Intern. Conf. on the Physics of Semiconductors, Edinburgh, Inst. of Phys. Conf. Series 43 (1979) 1343.
- [27] D.C. Tsui, A. Kamgar and M.D. Sturge, in: ref. [26], p. 1335.
- [28] M. Nakayama and L.J. Sham, in: ref. [26], p. 1339.
- [29] F.J. Ohkawa and Y. Uemura, J. Phys. Soc. Japan 43 (1977) 907, 933.
- [30] F.J. Ohkawa, J. Phys. Soc. Japan 45 (1978) 1427.
- [31] W. Sesselmann and J.P. Kotthaus, to be published.
- [32] A. Kamgar, M.D. Sturge and D.C. Tsui, to be published.